Diffuse reflection imaging of sub-epidermal tissue haematocrit using a simple RGB camera

Martin J. Leahy[a*], Jim O'Doherty[a], Paul McNamara[a], Joakim Henricson[b], Gert E. Nilsson[c,d], Chris Anderson[b] and Folke Sjoberg[b]

[a] Department of Physics, University of Limerick, National Technological Park, Ireland;
[b] Dept. of Biomedicine and Surgery, Linköping University Hospital, Linköping, S-581 85, Sweden;
[c]Dept. of Biomedical Engineering, Linköping University, Linköping, S-581 85, Sweden;
[d]WheelsBridge AB, Lövsbergsvägen 13, S-589 37, Linköping, Sweden.

ABSTRACT

This paper describes the design and evaluation of a novel easy to use, tissue viability imaging system (*TiVi*). The system is based on the methods of diffuse reflectance spectroscopy and polarization spectroscopy. The technique has been developed as an alternative to current imaging technology in the area of microcirculation imaging, most notably optical coherence tomography (OCT) and laser Doppler perfusion imaging (LDPI). The system is based on standard digital camera technology, and is sensitive to red blood cells (RBCs) in the microcirculation. Lack of clinical acceptance of both OCT and LDPI fuels the need for an objective, simple, reproducible and portable imaging method that can provide accurate measurements related to stimulus vasoactivity in the microvasculature. The limitations of these technologies are discussed in this paper. Uses of the Tissue Viability system include skin care products, drug development, and assessment spatial and temporal aspects of vasodilation (erythema) and vasoconstriction (blanching).

Keywords: Diffuse reflectance spectroscopy; polarization spectroscopy; microcirculation imaging; optical coherence tomography (OCT); laser Doppler perfusion imaging (LDPI); inflammation; blood flow

1. INTRODUCTION

Skin microvasculature is extremely complex in structure. It has previously been determined that there are on the order of 10^{10} blood vessels in the human body which have comparable dimensions with an RBC, which constitutes approximately 19,000 km of human blood vasculature[1], requiring 9% of total cardiac output even in resting conditions[2]. Lying just under the epidermis at approximately 150 μm from the skin surface is the upper papillary dermal matrix, which contains the nutritional blood vessels and arterio-venous anastomoses (AVA's). Beneath this layer lies the reticular dermis which is composed of arterioles, venules and firm connective tissue. Changes in arteriole blood flow is controlled by the autonomic nervous system, and this in turn controls the blood flow through the nutritional capillaries, leading to an increase or decrease of blood flow.

Due to the extraordinarily large amount of blood vessels in the microcirculation with similar dimensions to an RBC, it is highly probable that a defect in the local circulatory system will occur in microvessels in the immediate area. Defects will become extremely dangerous in a sensitive organ such as in the eyes or ears. Abnormal cutaneous blood flow can indicate serious conditions in organs not close to the skin and if a constant flow of blood does not keep pace with metabolism, tissue necrosis can occur. Many diseases begin at cellular level and most physicians believe that the first signs of those diseases appear as changes in the microcirculation. Recent research has also explored the possible link between skin microcirculation

* Further author information: (Send correspondence to Martin Leahy)
Martin Leahy.: E-mail: martin.leahy@ul.ie , Telephone: +353 61 213056
Gert E. Nilsson.: E-mail: info@wheelsbridge.se Telephone: +46 708 765 190

dysfunction and coronary heart disease[3], as well as the blood flow within and outside skin cancers[4]. Even though this may be true, no method of microcirculation imaging has yet supplanted the awkward and qualitative method of clinical observation for diagnosis of microvasculature conditions.

Imaging of tissue perfusion is an extremely important tool in assessing the influence of peripheral vascular disease in the human microcirculation. It is of utmost importance in the diagnosis of various conditions to be able to measure the flow or concentration in relatively small areas of tissue, rather than in the capillary bed as a whole, in order to pinpoint specifically affected areas. Thus significant spatial resolution in the tissue is required, and this resolution is variable with the amount of scattering and absorption presented by the tissue. Many clinical conditions that affect the microcirculation of the skin are still diagnosed and followed-up by observational methods alone in spite of the fact that non-invasive, more user-independent and objective methods are available today. Limited portability, high cost, lack of robustness and non-specificity of findings are among the factors that have hampered the implementation of these methods in a clinical setting. The ideal blood flow monitor should be objective, non-invasive, and capable reproducible readings. Image acquisition should be instantaneous, to reduce the misrepresentation of temporal variations as spatial heterogeneity in the tissue RBC concentration. In addition, it should be able to give values for perfusion, which are independent of tissue characteristics such as thickness, capillary density and optical properties. The latter is especially important when considering the varying amounts of melanin presented by inter-individual skin, since melanin will act as an absorption filter and modulate the light transmitted to the papillary dermis. Patient motion has been known to affect results in all microcirculation evaluation techniques, and has been addressed with the technology presented in this paper.

2. LASER DOPPLER PERFUSION IMAGING (LDPI)

In 1972 Riva and co-workers[5] were the first to develop an instrument to measure RBC velocity in a glass flow tube model. By 1975 Stern[6] had demonstrated that Doppler shifted laser light could be used to analyse RBC movement in the skin tissues. The single-point measurement laser Doppler perfusion monitor (LDPM) became a commercially available research tool[7] and with the onset of home computers and increased computing power, led to the construction of a multi-point measurement imager in 1993[8]. A laser Doppler image is simply an image in which the perfusion has been measured at individual points and placed together on a pseudo-colour map, which is the best method for presenting many single point measurements together[8].

The persistent lack of clinical acceptance for LDPI arises from the limitations of the technique. Limitations for LDPI include:

- Lack of an absolute zero measurement. Previously this had been attributed to Brownian motion within the vascular compartment and RBC vasomotion[9, 10], but more recently has been also attributed to the Brownian motion of macromolecules arising from the interstitial compartment[11].
- Restricted measurements of 1 mm^2 at a time, sensitivity to motion and vibration with poor reproducibility of readings[12].
- Lack of knowledge of sampling depth in the tissue.
- Mechanical steering of the laser beam takes substantial time, and temporal effects can be mis-interpreted as spatial heterogeneity in the microvasculature. A standard LDPI takes 20 seconds to capture an image of 64x64 pixels.

Steps have been taken in recent years to reduce these limitations to a clinically acceptable level. The laser beam area can be reduced to 40μm with a step size of 25 μm using enhanced resolution LDPI (EHR-LDPI), leading to an axial spatial resolution of 0.47 mm for 4096 points compared to 0.97 mm for 1024 points for a standard imager[13]. This axial resolution along with the reduced laser beam area allows the EHR-LDPI to image perfusion in single microvessels. More recently, Moor Instruments (Axminster, UK) have developed a line scanning laser Doppler imager. This reduces image acquisition time, since the imager acquires a horizontal line of 64 data points instantaneously and then moves to the next vertical position, sweeping across the tissue. Imaging time is now reduced to 5 seconds for a 50x64 pixel image[14].

Recently, a method of LDPI has been developed that does not use the raster scan method, but can acquire the Doppler information 4 times faster than conventional scanning technology[15]. This method is called parallel LDPI, whereby mechanical scanning is substituted by a full-field photoelectrical scan with a divergent laser beam of 20-40 mm, resulting in a faster acquisition speed. Photodetection in parallel LDPI is performed with a 2D matrix of photodetectors on a CMOS image

sensor (an intelligent camera). This technique's best imaging time so far has been 5 seconds for a 64x64 pixel image, compared to a commercial unit taking 20 seconds for the same size pixel image[16]. *In vivo* hypoxic occlusion in the index finger has proven to be distinguishable with this new system. Fig. 1 details the differences in the operation between the serial and parallel versions of LDPI. This parallel progression of LDPI will facilitate real-time acquisition in the future, as the fastest refresh rate is currently 90 seconds from data acquisition to image production on the screen[17], while conventional LDPI refresh rate is on the order of minutes.

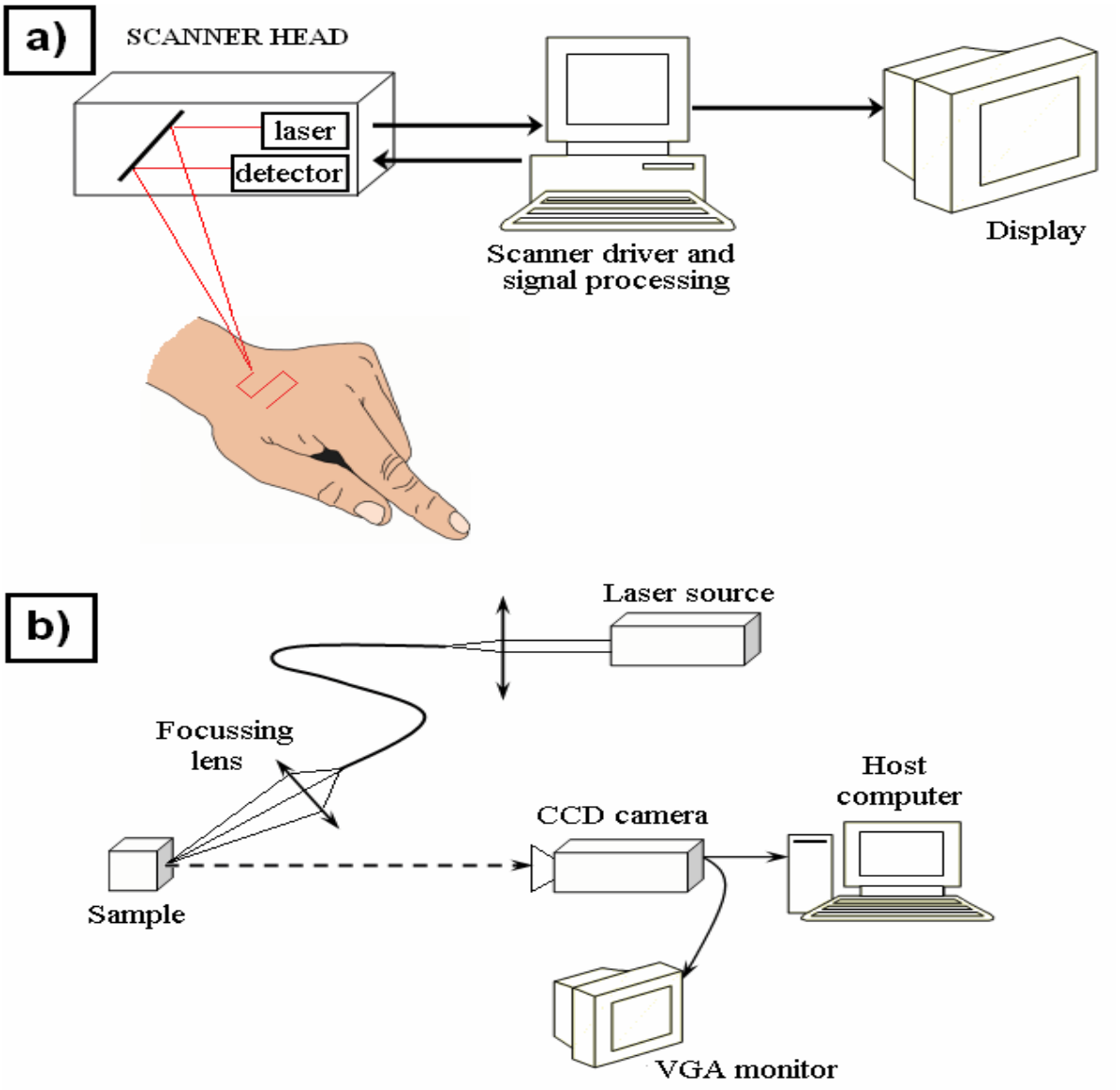

Figure 1 Experimental setup of serial LDPI (a) showing the rastering fashion of the scanner on the subjected area and parallel LDPI (b) showing larger area illumination and detection by CCD camera. The beam is increased to a diameter of 20-40 mm, compared to a beam diameter of approximately 2 mm for serial LDPI.

Recent efforts in standardising both LDPM and LDPI have been in progress, a standard perfusion unit as well as a single calibration procedure should be in use across Europe in order to make comparable measurements[18]. In 2002, a report on a project named HIRELADO (HIgh REsolution LAser DOppler) from the standardisation group of the European society of contact dermatitis published guidelines on the measuring of skin blood flow, addressing mainly technical aspects and image interpretation. They bypassed they problem of the perfusion units simply by all international groups involved in the project using the same commercial instrument (Lisca AB, Sweden), and if HR-LDPI is to be carried out, then these guidelines should be followed closely. Between 1997 and 2002 a standardisation project was undertaken by many international research institutes and manufacturers, in which a perfusion simulator for calibration and standardisation of LDPM and use of nomenclature was agreed. Results of this study have still not formally established scaling factors between different companies standardised instruments as well as standardised protocol for LDPM devices.[19]

3. OPTICAL COHERENCE TOMOGRAPHY

First developed by Huang in 1991[20], optical coherence tomography (OCT) is an imaging technique which provides high resolution cross sectional images of biological structures. Its major uses so far have been in ophthalmology and imaging in the retinal area to diagnose a variety of macular diseases[21] and choroidal tumours[22], due to the retina's weak scattering properties. In highly scattering media, the light beam is rapidly attenuated with propagation depth, resulting in signal degradation. It provides a method of "optical biopsy" on a similar resolution scale as histopathology. The technology derives much fibre-based instrumentation from the telecommunications industry, taking advantage of a well-developed modular technology base. Image resolution is usually in the area of 1-15 μm, which is one or two orders higher than that of ultrasound imaging, and in some cases can have resolution similar to 100 x magnification histology examination. The delay in application to other *in vivo* tissue structures has been mainly due to the problem of the sampling depth, which largely excludes broadband sources from deep subsurface imaging. Even though this effect is noted, OCT has recently been applied to the sensitive area of measuring glucose levels non-invasively in human blood[23].

OCT requires no direct contact with the tissue under investigation, and backscattered light from a tissue sample is interfered with by a reference wave in a technique called low-coherence interferometry. On observation of Fig. 2, the light from the reference and sample arms interferes at the detector only when the difference of their path lengths is within the coherence length of the light source. The depth of measurement is controlled by "scanning" the reference arm at a constant velocity v so that the light travels a further distance of up to 1 mm. After interacting with the biological sample, the reference beam which has undergone no interaction and the sample beam are recombined at an optical detector. IR sources with wavelength greater than 1000 nm are normally used since ocular media are essentially transparent at this wavelength, thus providing optical access to the anterior eye chamber and of course, the retina.

A major limiting factor for optical imaging of tissues is the absorption of water, which significantly deteriorates tissue transparency at wavelengths in the region of 1–2 μm. However, in most biological tissues, scattering in the near infrared wavelength region is one or two orders of magnitude higher than absorption. Therefore, OCT penetration in biological tissue tends to increase with increasing wavelength from hundreds of microns in the shorter wavelength region of the visible spectrum (about 450–550 nm) to about 1–2 mm in the mid infrared (1300–1500 nm) [24].

OCT images of skin tissue provide merely physical examination of the first 1 mm of the tissue Arteries and veins have been distinguished in deeper tissues by applying Doppler algorithms to distinguish flow directions and speed[25], but no spectroscopic information about blood in the microvascular network or any other chromophore can be obtained.

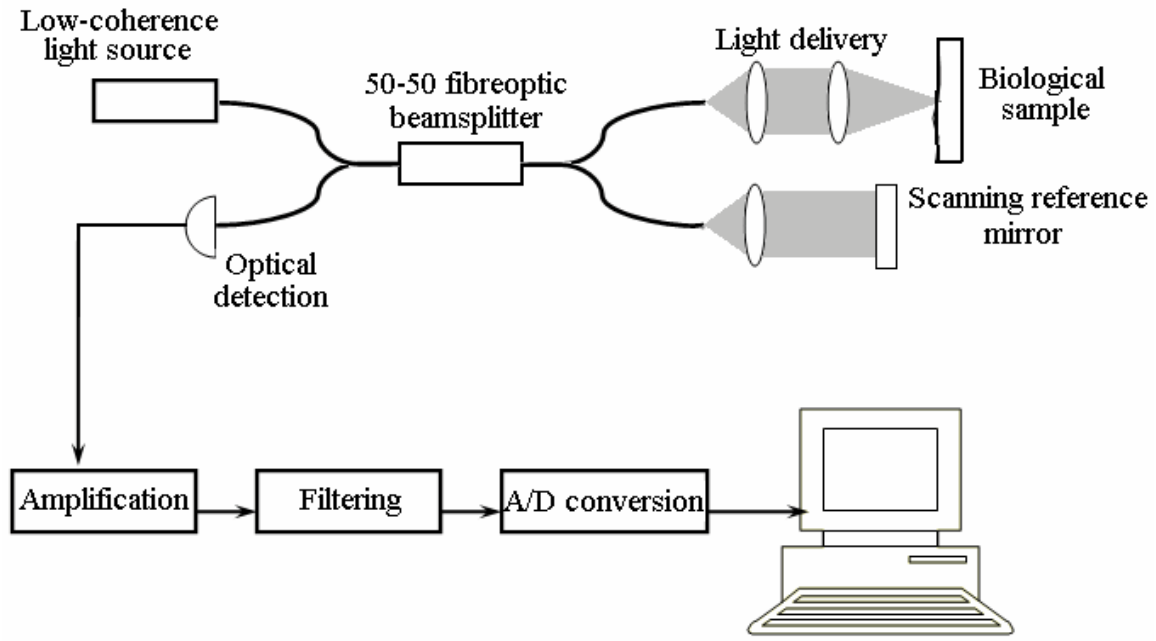

Figure 2. Instrumentation detailing the operation of an OCT system20. Due to the interconnectivity of fibre-based instruments, OCT can be integrated with many instruments, and light delivery can be carried out via cathethers26, microscopes27, ophthalmoscopes or endoscopes.

4. DIFFUSE REFLECTANCE POLARIZATION IMAGING

It is widely recognized that the original polarization state is lost in multiply scattered light, although it may be partially preserved in weakly scattered light. Thus it is possible to use polarization techniques to image areas where weak scattering is prevalent, such as in the superficial layers of the skin. The study of light scattering by *Bacillus subtilis* (bacterium) introduced the first medical polarization examining techniques[28], although the first observation of rejecting the surface glare by viewing the skin through polarizing filters oriented perpendicular to the incident light was reported by Anderson[29]. Although still a relatively small area as regards to tissue imaging technologies, many papers have been published citing the use of polarization imaging for cancer boundary detection[30,31], optical properties determination of diseased and control tissues[32], examination of lentigo[33] and visualization of water content in the skin[34]. The concept of polarization tissue imaging received a theoretical boost when it was suggested that reflected polarized imaging in skin would not suffer significant blurring, and therefore imaging of the superficial layers of skin was possible without much loss of information[35].

Polarized light studies are not applicable to the investigation of thick tissues, since the polarization information is lost after relatively few scattering events following the migration of photons into the tissue. It is, however, useful for analysis of light backscattered from thin, layered scattering media such as the epidermal layers of the skin. The methodology of subsurface polarization light spectroscopy involves illuminating the skin with incoherent light polarized by a linear polarizing filter, and observing the backscattered light through another linear polarizing filter with its pass direction oriented perpendicular to the direction of the illumination light. Light enters the tissue and is rapidly depolarized by scattering events and tissue birefringence due to collagen fibers. Thus, the light backscattered from the skin consists of both polarized and randomly polarized light, and so the polarized component (which has only interacted with the superficial epidermal layers) is blocked by the second polarizing filter. A portion of the randomly polarized light passes through the second filter, and reaches a CCD detection array. The effects of rotating the detection polarizer is shown in Fig. 3.

Monte Carlo methods of modelling the propagation of polarized light through the skin,[36, 37] and experimental validation[38, 39] have detailed the sampling depth of linearly polarized light to be in the order of 5-10 scattering mean free path lengths[40, 31] and is dependent on the optical properties of the sample for wide-area tissue imaging[41]. The average sampling depth in skin tissue amounts to approximately 500 μm at a wavelength of 633 nm, which is well into the reticular dermis where light is diffusely scattered and absorbed by the hemoglobin molecule in the RBCs and by other tissue constituents.

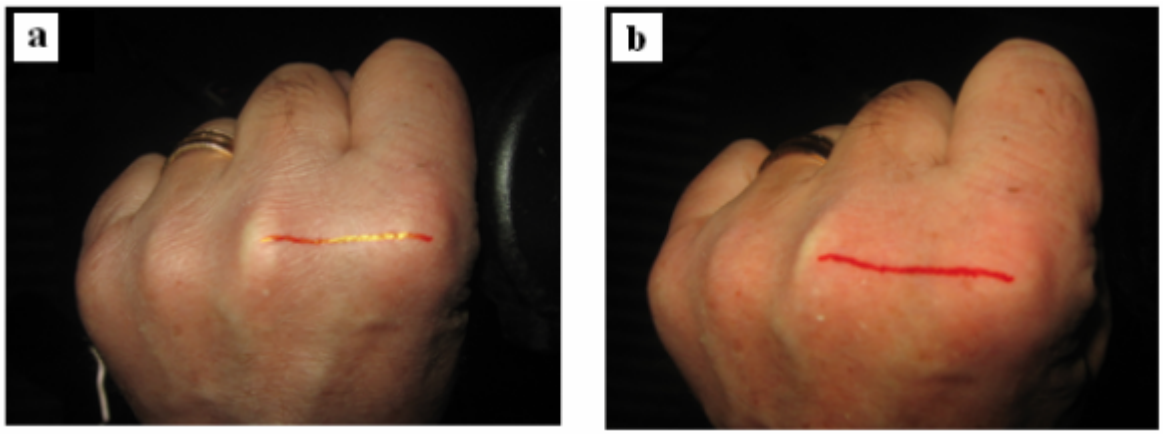

Figure 3. Images acquired with polarization filters (a) parallel and (b) perpendicular (a) show reflections from the surface layers of skin, and the red colour produced by underlying layers is not evident due to skin surface detail, while (b) shows a reddish colour indicating subsurface imaging, and shows no information about the surface layers such as wrinkles. A red line drawn on the skin shows specular reflection in some places in (a), while there is no specular reflection in (b). Reflections from the surface of the gold ring are also suppressed in (b).

5. SYSTEM THEORY

The system theory is already described by O'Doherty *et al.* [43], but is provided here for completeness. Linearly polarised light is almost completely depolarised at a depth of approximately 300 μm, which is a substantial distance into the reticular dermis in most skin sites. In this section of tissue, light is diffusely scattered and absorbed by the RBCs in the microvascular blood vessels, and other tissue structures (such as skin cells, hair follicles) present in this compartment. Broadband incoherent wide-angle light is provided by the camera flash, and the image is acquired instantaneously. The operation of the system detailed in Fig. 4 shows the linear and depolarized light components and how the signal is filtered to create a diffuse reflection polarized image.

When light is incident on the skin surface, approximately 5% is reflected as surface glare, while a further 2% is reflected from subsurface superficial tissues. These 2 reflections retain their polarization states. Approximately 53% is absorbed into the skin matrix and is not re-emitted in any direction. Thus the backscattered light amounts to 40% of the incident light, which penetrates into the dermal area of the skin, and the polarization state is randomized by multiple scattering. Due to this randomization, approximately 20% is assumed to be parallel polarised and the other 20% is perpendicular polarised[42]. Thus the degree of polarization of the detected light is dependent on the incident polarization state, thickness and tissue optical properties. This technique is based on the assumption that weakly scattered light retains its polarization state, whereas multiply scattered light will depolarize faster.

Wavelengths of interest for papillary dermal imaging by our method are from 500 nm – 600 nm (green) and from 600 nm – 700 nm (red). Blue light from 400 nm – 500 nm is assumed to be absorbed by the epidermal melanin layer. Mathematical modelling of the system requires the use of standard optical properties for the tissue and its constituent chromophores, namely the absorption coefficient μ_a and scattering coefficient μ_s for Type II tissue. The refractive index of skin tissue and

haemoglobin is assumed to be constant. These values were obtained from literature[44, 45, 46] and a curve fitting model applied to interpolate the values for each wavelength. An average value of these for mathematical modelling is detailed in Table 1.

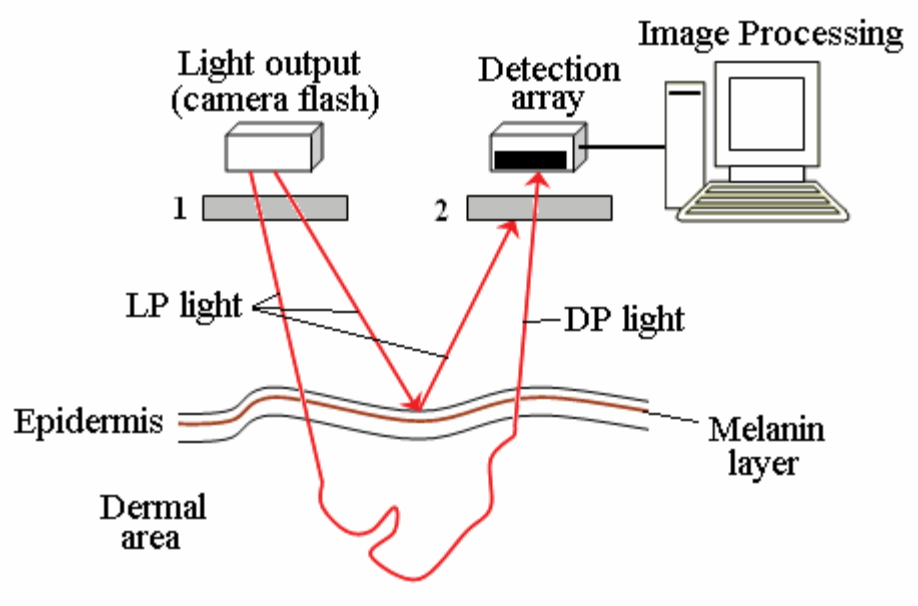

Figure 4. Operation of the *TiVi* system, showing the *polarization* discrimination method. Both 1 and 2 are polarization filters and are arranged so that their pass directions are perpendicular. By this method, the surface reflections are suppressed and only the light emanating from the dermal area is received by the detection array. LP and DP represent linear polarised and depolarised light respectively.

Table 1. Average approximate absorption (μ_a) and scattering (μ_s) coefficients in cm^{-1} for various chromophores in human skin tissue for the red and green wavelength region. The values were averaged by applying an interpolation curve to the existing data from literature [44, 45, 46]. Note that oxygenation of the RBC has no effect on its scattering properties.

Absorber	**Red (600 -700 nm)**		**Green (500 – 600 nm)**	
	$\mu_a(\Delta\lambda_r)$	$\mu_s(\Delta\lambda_r)$	$\mu_a(\Delta\lambda_g)$	$\mu_s(\Delta\lambda_g)$
Tissue	2.7	187	3	223
RBC_{oxy}	3.5	861	177	920
RBC_{deoxy}	25	861	201	920
Epidermis	35	450	40	535

5.1 Mathematical Derivation

The wavelength-dependent intensity of backscattered light with a perpendicular polarization to the incident polarized light is described by the equation[42]:

$$I_{per}(\Delta\lambda) \propto k_0(\Delta\lambda) I_0 T_{epid}(\Delta\lambda) R_d(\Delta\lambda) \quad \textbf{(1)}$$

where $k_0(\Delta\lambda)$ represents the fraction of the total emitted light intensity I_0 within the wavelength interval $\Delta\lambda$, impinging on the skin, $T_{epid}(\Delta\lambda)$ represents transmission properties of the epidermal layer, and $R_d(\Delta\lambda)$ represents diffusely reflected light in the reticular dermis. In order to quantify the fraction of RBCs in the tissue microvasculature as an expression of the viability of the tissue, an algorithm is suggested that does not depend on the total light intensity and takes advantage of the fact that green light is absorbed to a higher degree in RBCs than red light, while light in both wavelength regions is absorbed to a comparatively low and similar degree by the surrounding tissue. The tissue viability index ($TiVi_{index}$), is defined as:

$$TiVi_{index} = k_{gain}\left(\frac{I_{per}(\Delta\lambda_r) - k_1 I_{per}(\Delta\lambda_g)}{I_{per}(\Delta\lambda_r)}\right) \quad \textbf{(2)}$$

where $I_{per}(\Delta\lambda_r)$ and $I_{per}(\Delta\lambda_g)$ represent the perpendicularly oriented and wavelength-dependent intensity of backscattered light in the red and green wavelength regions. The constant k_1 can be fitted for best algorithm performance, and k_{gain} is a constant that represents the gain factor. Inserting Eqn. 1 into Eqn. 2 cancelling the I_0 factor and setting $k = k_1 k_0(\Delta\lambda_g) / k_0(\Delta\lambda_r)$, the algorithm is expanded to:

$$TiVi_{index} = k_{gain}\frac{T_{epid}(\Delta\lambda_r) R_d(\Delta\lambda_r) - k T_{epid}(\Delta\lambda_g) R_d(\Delta\lambda_g)}{T_{epid}(\Delta\lambda_r) R_d(\Delta\lambda_r)} \quad \textbf{(3)}$$

The independence of total light intensity in the algorithm employed implies that the $TiVi_{index}$ calculated is only minimally influenced by the distance to and the curvature of the area under examination. Incident and diffusely backscattered light will pass through the epidermal melanin layer, thus the volume fraction of melanin will modulate the amount of backscattered light. The melanin layer can be thought of as an absorption filter, and its spectral characteristics show an exponential decrease of absorption with wavelength. For a sufficiently thin melanin layer, T_{epid} can be approximated to 1, reducing the algorithm to:

$$TiVi_{index} = k_{gain}\left(\frac{R_d(\Delta\lambda_r) - k R_d(\Delta\lambda_g)}{R_d(\Delta\lambda_r)}\right) \quad \textbf{(4)}$$

According to Kubelka-Munk theory[47] and its modification[48] the wavelength-dependent diffusely reflected light from a slab of infinite length can be expressed as:

$$R_d(\Delta\lambda) = 1 + \frac{K(\Delta\lambda)}{S(\Delta\lambda)} - \left(\frac{K(\Delta\lambda)^2}{S(\Delta\lambda)^2} + 2\frac{K(\Delta\lambda)}{S(\Delta\lambda)}\right)^{1/2} \quad \textbf{(5)}$$

where K and S are Kubelka-Munk absorption and scattering coefficients. Using a derivation from diffusion theory [48, 49] and assuming isotropic scattering, it can be shown that:

$$R_d(\Delta\lambda) = 1 + \frac{8\mu_a(\Delta\lambda)}{3\mu_s(\Delta\lambda)} - \left(\frac{(8\mu_a(\Delta\lambda))^2}{(3\mu_s(\Delta\lambda))^2} + 2\frac{8\mu_a(\Delta\lambda)}{3\mu_s(\Delta\lambda)} \right)^{1/2} \quad \textbf{(6)}$$

where $\mu_a(\Delta\lambda)$ is the absorption coefficient and $\mu_s(\Delta\lambda)$ is the scattering coefficient. The total absorption and scattering coefficients can each be considered to be composed of two parts – one that relates to the RBC ($\mu_{aRBC}(\Delta\lambda)$ and $\mu_{sRBC}(\Delta\lambda)$) and one that relates to the remaining tissue ($\mu_{aTISSUE}(\Delta\lambda)$ and $\mu_{sTISSUE}(\Delta\lambda)$). The total tissue absorption $\mu_a(\lambda)$ and scattering coefficient $\mu_s(\lambda)$ can be regarded as a linear combination of these two parts:

$$\mu_a(\lambda) = RBC_f \mu_{a\,RBC}(\lambda) + (1 - RBC_f)\mu_{aTISSUE}(\lambda) \quad \textbf{(7)}$$

$$\mu_s(\lambda) = RBC_f \mu_{s\,RBC}(\lambda) + (1 - RBC_f)\mu_{sTISSUE}(\lambda) \quad \textbf{(8)}$$

where RBC_f represents the volume fraction of RBCs occupying the tissue volume under consideration. Inserting numerical values from Table 1 results in a k value of 0.9905. The simulated non-linearized $TiVi_{index}$ is displayed as a function of RBC_f in Fig. 5 for the oxygen saturation levels 60%, and 100% demonstrating the relative independence from oxygen saturation.

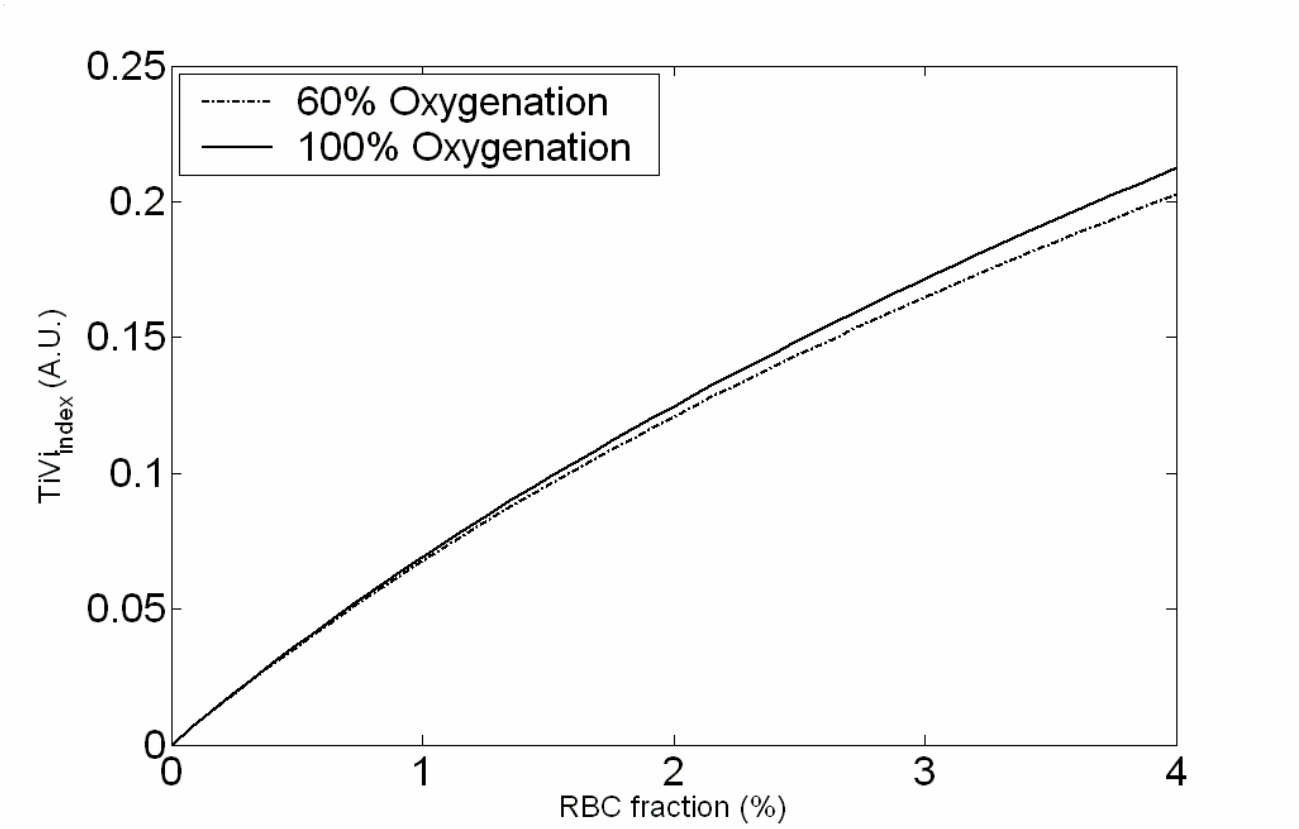

Figure 5. Simulated $TiVi_{index}$ for the values from Table 1 for 2 oxygenation levels, 60% and 100%.

The influence of a thin melanin layer in the epidermis can be modelled by way of an absorption filter with the transmission function:

$$T_{epid}(\Delta\lambda) = e^{-2\mu_{aEPID}(\Delta\lambda)x} \tag{9}$$

where μ_{aEPID} is the wavelength-dependent absorption coefficient of the epidermal layer and x is the layer thickness. Inserting Eqn. 9 into Eqn. 3 gives:

$$TiVi_{index} = k_{gain}\frac{R_d(\Delta\lambda_r) - ke^{-2(\mu_{aEPID}(\Delta\lambda_g)-\mu_{aEPID}(\Delta\lambda_r))x}R_d(\Delta\lambda_g)}{R_d(\Delta\lambda_r)} \tag{10}$$

In forearm skin where most skin testing is performed, the epidermal layer thickness amounts to 50 - 100 µm, resulting in a numerical value of $e^{-2(\mu_{aEPID}(\Delta\lambda_g)-\mu_{aEPID}(\Delta\lambda_r))x}$ of about 0.90 to 0.95 based on values inserted from Table 1.

6. INSTRUMEMTATION

A custom system was developed and is commercially available (WheelsBridge AB®, Linköping, Sweden) to examine RBC concentration in the papillary dermis of skin tissue by way of diffuse reflection polarization imaging. The system comprises of a consumer end digital camera containing a single CCD and Bayer colour filter array for filtering the red green and blue colour channels (Canon S80, Canon Inc., Japan). A polarization filter is placed over the flash (light source) and a filter of perpendicular pass direction is placed over the lens. The camera distance from the tissue surface for imaging is between 10 cm and 15 cm. The camera is connected to a PC by USB and controlled remotely by custom designed image processing software. All parameters of the camera can be controlled, such as image resolution, zoom, macro capabilities etc.

A series of images (captured in 8-bit RGB format) can be automated for capture by setting a time step for acquisition. This time step between images is a minimum of 5 seconds due to flash recycle time. A download folder and image sequence names can be automatically set by the user. Analysis software presented as a graphical user interface (GUI) was designed based on the theory detailed in the above section for analysis of the captured images. In a processed image (which we term a tissue viability image), RBC concentration is presented as a pseudo colour coded map, where red and blue colours represent high and low RBC concentration respectively. Many extra tools are available in the processing software such as the analysis of a region of interest from the sequence of images, creation of a movie from the images so as to compress and replay the dynamic changes in tissue viability that happen over several minutes to a time period of a few seconds. There is also an image aligning function that can align all the images to the same point, should the area under investigation move slightly during series acquisition. Statistical information for each image is displayed by default.

6.1 Image Processing Algorithm

Colour separation performed by the Bayer colour filter in the camera is repeated in the Matlab environment, with each image being separated into three colour planes, M_{red}, M_{green} and M_{blue}. By applying Eqn. 10 in the form:

$$\mathbf{M} = k_{gain} \frac{\mathbf{M}_{red} - k\mathbf{M}_{green}}{\mathbf{M}_{red}} \tag{11}$$

where $\mathbf{M}_{red}$, $\mathbf{M}_{green}$ are representative of $R_d(\Delta\lambda_r)$ and $R_d(\Delta\lambda_g)$ respectively. In order to compensate for the non-linear feature of the algorithm – the $TiVi_{index}$ - RBC_f relationship predicted by theory, each element in the M-matrix was further processed in accordance with:

$$\mathbf{M}_{out} = \mathbf{M}e^{-p*\mathbf{M}} \tag{12}$$

where p is an empirical factor fitted to produce best linear performance over the RBC interval of interest (0 – 4%). This was attained for a value of p = 2.6. The matrix (M_{out}) is presented as a two-dimensional pseudo-colour tissue RBC_f map, an example of which is presented in Fig. 6.

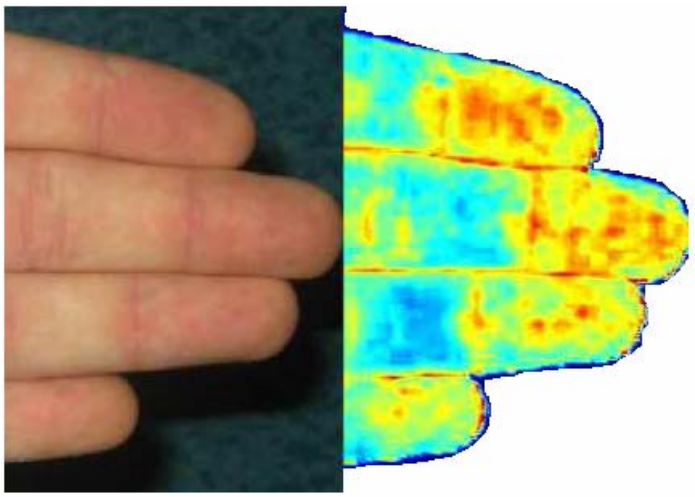

Figure 6. Example of the colour coded map generated by application of Eqn. 12. Note the non-homogenous distribution of blood in the fingertips.

7. *IN VIVO* EVALUATION

The designed system was used to investigate the microcirculation *in vivo* for externally applied stimuli. The effects of acetylcholine on the ventral forearm of young volunteers was studied. A circular iontophoresis electrode (i.d. 15 mm, height 3 mm) was attached and the well formed by the electrode was filled with acetylcholine diluted in physiological saline (10 mg/ml). After filling, the well was covered with a thin sheet of transparent glass and a pulsed current of 0.02 mA was fed through the electrode for 10 minutes. By this method, the positively charged acetylcholine molecules diffuse through the skin and reach the receptors in the microvascular network. The blood vessels dilate after interaction with the receptors, and an increase in tissue blood concentration occurs. One polarization spectroscopy image every 5 seconds was captured through the software, and processed. The average RBCf increase inside the well after 10 minutes was calculated to be 66%, and some areas had no response to the administered drug, while other areas varied by up to 117%. This shows the spatial heterogeneity of the 15 mm area. The before and after effects are detailed in Fig. 7.

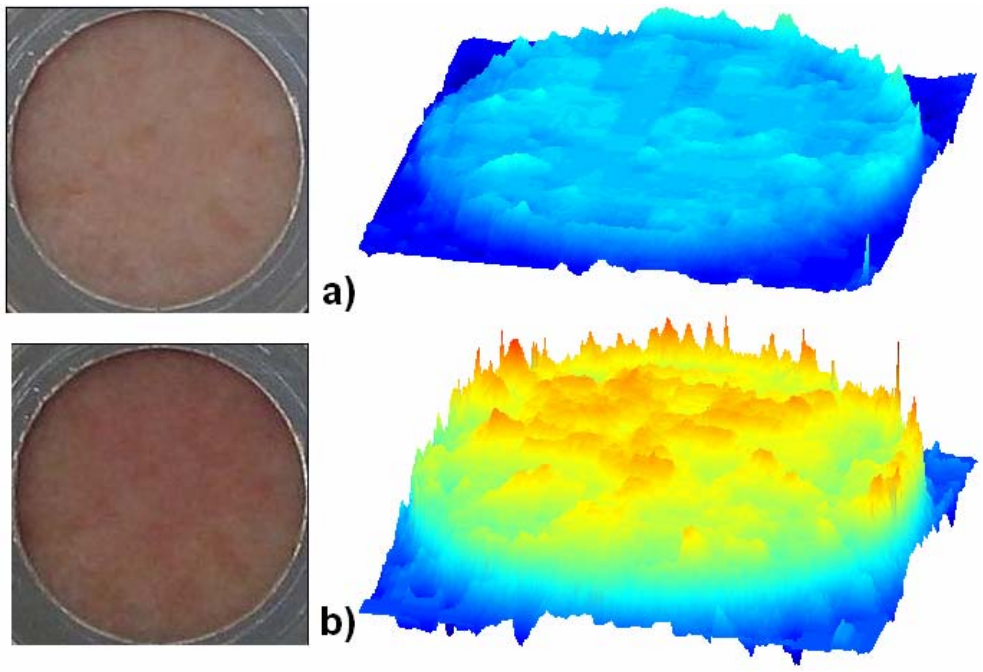

Figure 7. Before (a) and after (b) a 10 minute application of acetylcholine by iontophoresis. The processed images are rotated slightly to emphasise the $TiVi_{index}$ scale in the vertical direction.

A second *in vivo* test was carried out by applying clobestal propionate (0.5 mg/ml, Dermovat®, Glaxo Smith Kline, USA) to forearm skin in two quantities - 10 µl and 20 µl - at adjacent, round 20 mm diameter sites under occlusive cover (Tegederm™, 3M, St Paul, Minnsota, USA). The cover was removed after 12 hours and 20 µl methyl nicotinate (50 mmol) was applied topically on a third adjacent skin site. The three skin sites were expected to demonstrate erythema (vasodilatation) and blanching (vasoconstriction) respectively. The images displayed in Fig. 8 were recorded 10 minutes following application of methyl nicotinate and removal of the occlusion cover over the site exposed to clobestal propionate. The average $TiVi_{index}$ value for the methyl nicotinate site was calculated to be 30% above normal skin control levels. The average $TiVi_{index}$ for the the 20 µl and 10 µl clobestal propionate application sites were 31% respectively 19% below normal skin control levels.

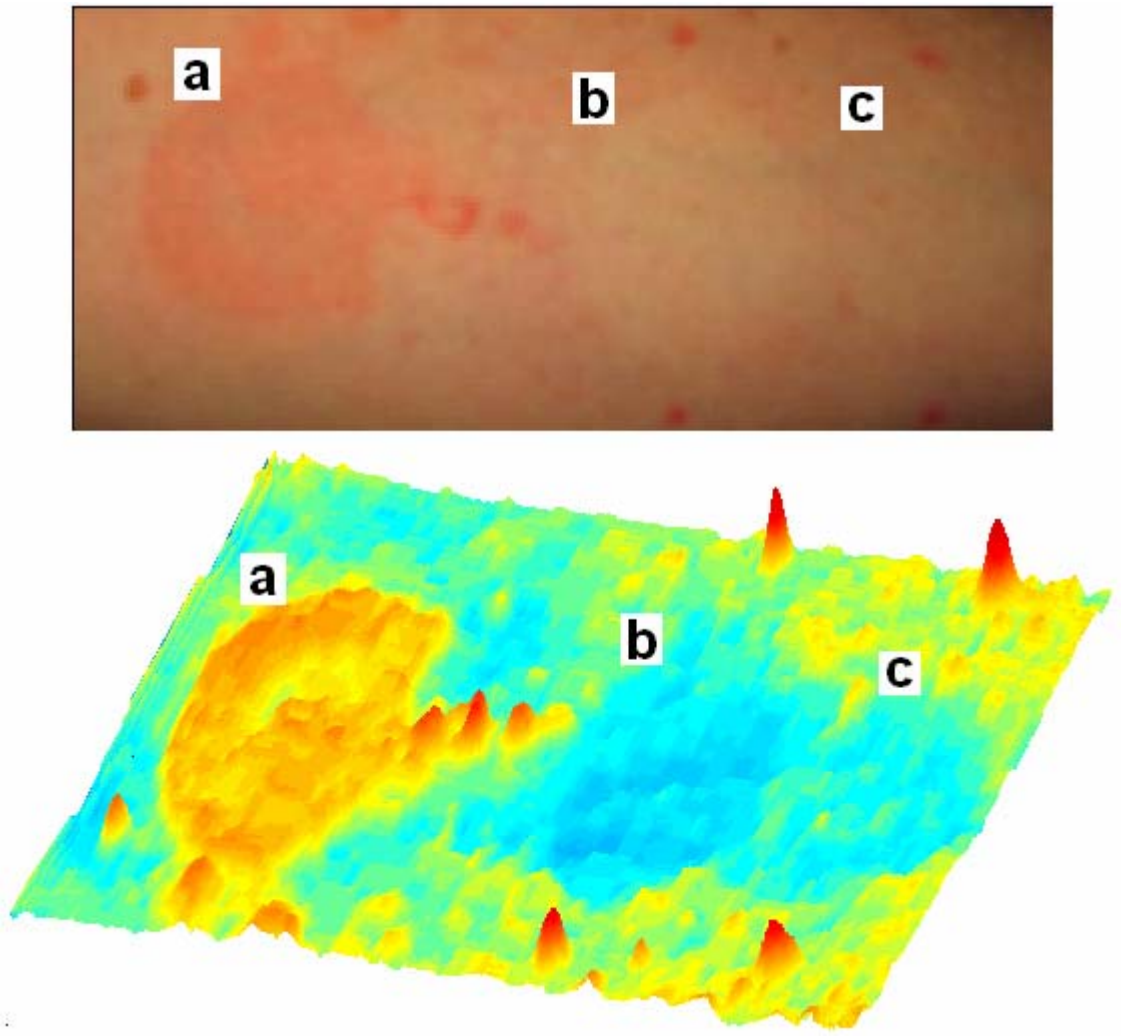

Figure 8. The after effects of a) methyl nicotinate b) clobestal propionate 20 µl and c) clobestal propionate 10 µl on successive skin sites. The processed image is rotated slightly to emphasise the $TiVi_{index}$ scale in the vertical direction.

8. CONCLUSIONS

A brief review of current research methods for investigating both the physical structure and microvascular RBC concentration has been given. Limitations of both of these techniques prompted further research into microvascular imaging, and the eventual design of a low-cost portable system to image RBC concentration in the papillary dermis. The system operates by polarization imaging, which suppresses the surface reflections from the skin surface, and only accepts light that has been diffusely backscattered from the deeper tissue. Theory developed by way of an adapted Kubelka-Munk model of the diffuse reflectance from dermal tissue was used via optical properties from literature. It should be noted that numerical values of tissue and blood optical properties are difficult to measure accurately, and the literature presents a wide range of values for these parameters, with variations of up to 100% in some cases[43]. Because the absorption of red light in tissue is relatively

independent of the amount of blood, the depth sensitivity is determined mainly by the penetration depth of the green light. This theory was used to propose an image processing algorithm, the performance of which was briefly evaluated, and a linear output between RBC concentration and system output was determined. The system has proven to be only slightly responsive to oxygen saturation, with only a small shift in $TiVi_{index}$ for a change in physiological extremes of 60% and 100%.

Two example tests of the system *in vivo* are described, firstly by the iontophoresis of acetylcholine on the forearm to produce vasodilation and secondly by the application of clobestal propionate and methyl nicotinate. The former application is of particular interest in the evaluation of peripheral neuropathy in diabetics, a patient group known to possess a weaker or even absent response to acetylcholine[50], and also in other assessment of reactive status of the microvasculature e.g. in severe burns or intensive care patients. The results show an important aspect of the system – the ability to quantify a decrease in the microvascular RBC concentration from normal levels. Additionally, since image acquisition is instantaneous, rapid changes such as the urticarial time course of methyl nicotinate reaction can easily be documented as images rather than single point measurements, thereby making it possible to simultaneously investigate both temporal and spatial aspects of rapid skin microvascular reactions. Extension of the technology to real-time video imaging at a frame rate of 5 Hz is underway.

ACKNOWLEDGMENTS

This research is supported in part by IRCSET (project RS/2003/135), the Irish Research Institute for Science, Engineering and Technology, and by VINNOVA (projects P26825-1 and P27840-1), the Swedish agency for Innovation Systems.

REFERENCES

1. R. A. Freitas, *Nanomedicine Vol. 1: Basic Capabilities*, Landes Bioscience, Georgetown, TX, USA, 1999.
2. G. J. Tortora and S. R. Grabowski, *Principles of Anotomy and Physiology*, *9 ed*., Wiley and Sons Inc., New York, NY, USA, 2000.
3. R. G. Ijzerman, R. T. de Jongh, M. A. M. Beijk, M. M. van Weissenbruch, H. A. Delemarre-van de Waal, E. H. Serne, and C. D. A. Stehouwer, "Individuals at increased coronary heart disease risk are characterized by an impaired microvascular function in skin," *Eur. J. Clin. Invest.*, vol. 33, pp. 536–542, 2003.
4. C. M. Choi and R. G. Bennett, "Laser Dopplers to determine cutaneous blood flow," *Dermatol. Surg.*, vol. 29, pp. 272 – 280, 2003.
5. C. Riva, B. Ross, and G. B. Benedek, "Laser Doppler measurements of blood flow in capillary tubes and retinal arteries," *Invest. Ophthalmol.*, vol. 11, pp. 936 – 944, 1972.
6. M. D. Stern, "*In Vivo* evaluation of micro-circulation by coherent light scattering," *Nature*, vol. 254, pp. 56-58, 1975.
7. G. E. Nilsson, T. Tenland, and P. A. Öberg, "A new instrument for continuous measurement of tissue blood blow by light beating spectroscopy," IEEE Trans. Bio-Med. Eng., vol. 27, pp. 9–12, 1980.
8. K.Wårdell, A. Jakobsson, and G. E. Nilsson, "Laser Doppler perfusion imaging by dynamic light scattering," *IEEE T. Bio-Med Eng.*, vol. 40, pp. 309–316, 1993.
9. P. Sullivan, G. A. Cioffi, L. Wang, C. A. Johnson, E. M. van Buskirk, K. R. Sherman, and D. R. Bacon, "The influence of ocular pulsatility on scanning laser Doppler flowmetry," *Am. J. Ophthalmol.*, vol. 128, pp. 81–87, 1999.
10. S. Bornmyr, H. Svensson, B. Lilja, and G. Sundkvist, "Skin temperature changes and changes in skin blood flow monitored with laser Doppler flowmetry and imaging: A methodological study in normal humans," *Clin. Physiol.*, vol. 17, pp. 71–81, 1997.
11. D. P. Kernick, J. E. Tooke, and A. C. Shore, "The biological zero in laser Doppler fluximetry: Origins and practical implementations," *Pfugers Arch.*, vol. 437, pp. 624–631, 1999.
12. W. L. Hickerson, S. L. Colgin, and K. G. Proctor, "Regional variations of laser Doppler blood flow in ischaemic skin flaps," *Plast. Reconsr. Surg.*, vol. 86, pp. 319–326, 1990.
13. M. Lindén, H. Golster, S. Bertuglia, A Colantuoni, F. Sjöberg and G. Nilsson, "Evaluation of enhanced high resolution laser Doppler imaging (HER-LDI) in an in vitro tube model with the aim of assessing blood flow in separate microvessels," Microvasc. Res., vol. 56, pp. 261–270, 1998.
14. Europe Patent No: EP0904011

15. A. Serov, W. Steenbergen, and F. de Mul, "Laser Doppler perfusion imaging with a complimentary metal oxide semiconductor image sensor," *Opt. Lett.*, vol. 27, pp. 300 – 302, 2002.
16. http://www.moor.co.uk/support/theory
17. A. Serov, B. Steinacher, and T. Lasser, "Full-field laser Doppler blood-flow imaging and monitoring using an intelligent cmos camera and area illumination," in *Saratov Fall Meeting 2004: Optical Technologies in Biophysics and Medicine*, Proc. SPIE 5771, pp. 95–102, 2005.
18. M. J. Leahy, F. F. de Mul, G. E. Nilsson, and R. Maniewski, "Principles and practice of the laser Doppler perfusion technique," *Technol. Health Care*, vol. 7, pp. 143–162, 1999.
19. European Project SMT4-CT97-2148, "Standardised calibration methods and europrobes for laser Doppler monitoring and imaging of blood perfusion in tissue," 1997-2002.
20. D. Huang, E. A. Swanson, C. P. Lin, J. P. Schuman, W. G. Stinson, W. Chang, M. R. Hee, T. Flotte, K. Gregory, C. A. Puliafito, and J. G. Fujimoto, "Optical coherence tomography," *Science*, vol. 254, pp. 1178–1181, 1991.
21. C. A. Puliafito, M. R. Hee, C. P. Lin, E. Reichel, J. S. Schuman, J. S. Dukar, J. A. Izatt, E. A. Swanson, and J. G. Fujimoto, "Imaging of macular diseases with optical coherence tomography," *Ophthalmolpgy*, vol. 102, pp. 217–229, 1995.
22. U. Schaudig, A. Hassenstein, A. Bernd, A. Walter, and G. Richard, "Limitations of imaging choroidal tumours *in vivo* by optical coherence tomography," *Graefe's Arch. Clin. Exp. Ophthalmol.*, vol. 236, pp. 588–592, 1998.
23. K. Larin, M. Motamedi, M. S. Eledrisi, and R. O. Esenaliev, "Noninvasive blood glucose monitoring with optical coherence tomography," *Diabetes Care*, vol. 25, pp. 2263–2267, 2002.
24. A. Unterhuber, B. Povazay, K. Bizheva, B. Hermann, H. Sattmann, A. Stingl, T. Le, M. Seefeld, R. Menzel, M. Preusser, H. Budka, C. Schubert, H. Reitsamer, P. K. Ahnelt, J. E. Morgan , A. Cowey and W. Drexler, "Advances in broadband light sources for ultrahigh resolution optical coherence tomography," *Phys. Med. Biol.*, vol. 49, pp. 1235–1246, 2004.
25. V. Yang, A. Vitkin, M. Gordon, A. Mok, L. Wongkeesong, P. Muller, N. Marcon, S. Mintz and B. Wilson, "UltraLIGHT: New frontiers of medical imaging", Univ. Toronto Medical Journal, vol 78, pp. 68–70, 2000.
26. N. V. Ifitimia, B. Bouma, J. F. deBoer, B. H. Park, B. Cense, G. J. Tearney, "Adaptive ranging for optical coherence tomography", *Opt. Express*, vol. 12, pp. 4025–4034, 2004.
27. A. Dubois, G. Moneron, K. Grieve and A. C. Boccara, "Three-dimensional cellular-level imaging using full-field optical coherence tomography," *Phys. Med. Biol.*, vol. 49, pp. 1227–1234, 2004.
28. W. S. Bickel, J. F. Davidson, D. R. Huffman, and R. Kilkson, "Application of polarization effects in light scattering: A new biophysical tool," *Proc. Natl. Acad. Sci. USA*, vol. 73, pp. 486–490, 1973.
29. R. R. Anderson, "Polarized-light examination and photography of the skin," *Arch. Dermatol.*, vol. 127, pp. 1000–1005, 1991.
30. J. C. Ramella-Roman, K. Lee, S. A. Prahl, and S. L. Jacques. "Design, testing and clinical studies of a handheld polarized light camera," *J. Biomed. Opt*. 9, pp. 1305–1310, 2004.
31. S. L. Jacques, J. C. Ramella-Roman, and K. Lee, "Imaging superficial tissues with polarized light," *Lasers Surg. Med.* vol. 26, pp. 119–129, 2000.
32. R. Nothdurft and G. Yao. "Expression of target optical properties in subsurface polarization-gated imaging," *Opt. Express* vol. 13, pp. 4185–4195, 2005.
33. S. P. Morgan and M. E. Ridgeway, "Polarization properties of light backscattered from a two layer scattering medium," Opt. Express, vol. 7, pp. 395–402, 2000.
34. H. Arimoto, "Visualization technique for water content distribution of skin tissue by dualband polarization imaging", in *Engineering in Medicine and Biology 27th annual conference*, Proceedings of the 2005 IEEE, pp. 3165–3168, 2005.
35. M. R. Ostermeyer, D. V. Stephens, L. Wang, and D. Stephens, "Nearfield polarization effects on light propagation in random media," in *OSA Topics on Biomedical Optical Spectroscopy and Diagnostics* , Vol. 3 of OSA Trends in Optics and Photonics Series, paper SP2, 1996.
36. X. Wang and L. V. Wang. "Propagation of polarized light in birefringent turbid media: A Monte Carlo study," J. *Biomed. Opt*. vol. 7, pp. 279–290, 2002.
37. Y. Liu, Y. L. Kim, X. Li and V. Backman, "Investigation of depth selectivity of polarization gating for tissue characterization," *Opt. Express*, vol. 13, pp. 601–611, 2005.

38. L. F. Rojas-Ochoa, D. Lacoste, R. Lenke, P. Schurtenberger and F. Scheffold, “Depolarization of backscattered linearly polarized light,” *J. Opt. Soc. Am. A,* vol. 21, pp. 1799–1804, 2004.
39. D. Bicout, C. Brossueu, A. S. Martinex and J. M. Schmitt, “Depolarization of multiply scattered waves by spherical diffusers: Influence of the size parameter,” *Phys. Rev. E*, vol. 49, pp. 1767–1770, 1994.
40. G. Jarry, E. Steimer, V. Damaschini, M. Epifanie, M. Jurczak, and R. Kaiser, “Coherence and polarization of light propagating through scattering media and biological tissues,” *Appl. Optics,* vol 37, pp. 7357–7367, 1998.
41. D. A. Zimnyakov and Y. P. Sinichkin, “A study of polarization decay as applied to improved imaging in scattering media,” *J. Opt. Pure. Appl. Opt*. vol. 2, pp. 2008, 2000.
42. S. L. Jacques, J. C. Ramella–Roman, and K. Lee, “Imaging skin pathology with polarized light,” *J. Biomed. Opt.*, vol. 7, pp. 329–340, 2002.
43. O’Doherty, J. Nilsson, G. E., Henricson, J. Sjöberg, F. and Leahy, M. J. Sub-epidermal imaging by polarised light rejection for assessment of microvascular patency. *Accepted for publication in: Skin Research and Technology* - Official journal of the International Society for Bioengineering Edited by: Jørgen Serup, 2007.
44. J. Mobley and T. Vo-Dinh, *Biomedical Photonics Handbook, ch. Optical Properties of Tissue*. CRC Press LLC, Boca Raton, USA, 2003.
45. I. V. Megliniski, and S. J. Matcher, “Computer simulation of the skin reflectance spectra,” *Comput. Meth. Prog. Bio.* Vol. 70, pp. 179–186, 2003.
46. S. Wray, M. Cope, D. T. Delpy, S. J. Wyatt and E. O. R. Reynolds, “Characterization of the near infrared absorption spectra of cytochrome aa3 and haemoglonin for the non-invasive monitoring of cerebral oxygen,” *Biochimica et Biophysica Acta* vol. 933, pp. 184–192, 1988.
47. A. Ishimaru *Wave Propagation and Scattering in Random Media, Vol. 1 Single scattering and transport theory*, Academic Press, London, 1978.
48. F. Fabbri, M. A. Francesschini and S. Fantini,. “Characterization of spatial and temporal variations in the optical properties of tissue-like media with diffuse reflectance imaging,” *Appl. Optics*, vol. 42, pp 3063–3072, 2003.
49. B. J. Brinkworth, “A diffusion model of the transport of radiation from a point source in the lower atmosphere,” *Brit. J. Appl. Phys.* vol. 15, pp. 733–741, 1964.
50. S. J. Morris and A. C. Shore, “Skin blood flow responses to the iontophoresis of acetylcholine and sodium nitroprusside in man: possible mechanism,” *J. Physiol*. October 15; 496(Pt 2): 531–542, 1996.